



UvA-DARE (Digital Academic Repository)

Dynamic light scattering studies on the sol-gel transition of a suspension of anisotropic colloidal particles

Kroon, M.; Wegdam, G.H.; Sprik, R.

DOI

[10.1103/PhysRevE.54.6541](https://doi.org/10.1103/PhysRevE.54.6541)

Publication date

1996

Published in

Physical Review E

[Link to publication](#)

Citation for published version (APA):

Kroon, M., Wegdam, G. H., & Sprik, R. (1996). Dynamic light scattering studies on the sol-gel transition of a suspension of anisotropic colloidal particles. *Physical Review E*, 54, 6541-6550. <https://doi.org/10.1103/PhysRevE.54.6541>

General rights

It is not permitted to download or to forward/distribute the text or part of it without the consent of the author(s) and/or copyright holder(s), other than for strictly personal, individual use, unless the work is under an open content license (like Creative Commons).

Disclaimer/Complaints regulations

If you believe that digital publication of certain material infringes any of your rights or (privacy) interests, please let the Library know, stating your reasons. In case of a legitimate complaint, the Library will make the material inaccessible and/or remove it from the website. Please Ask the Library: <https://uba.uva.nl/en/contact>, or a letter to: Library of the University of Amsterdam, Secretariat, Singel 425, 1012 WP Amsterdam, The Netherlands. You will be contacted as soon as possible.

Dynamic light scattering studies on the sol-gel transition of a suspension of anisotropic colloidal particles

Mark Kroon,* Gerard H. Wegdam, and Rudolf Sprik

Van der Waals-Zeeman Instituut, Universiteit van Amsterdam, Valckenierstraat 65, 1018 XE Amsterdam, The Netherlands

(Received 14 May 1996)

We present a dynamic light scattering study on the sol-gel transition of a suspension of disk-shaped colloidal particles in water. We obtain the static and fluctuating part of the scattered intensity, the fraction of frozen-in density fluctuations, and the intermediate scattering function from a local time-averaged measurement of the intensity correlation function and the scattered intensity. The sol-gel transition is marked by a drastic change in the static part of the scattered intensity. The intermediate scattering function shows a stretching of the translational correlation time over more than five orders of magnitude. In the gel phase the function shows a power-law decay, with a concentration dependent scaling exponent. Our results show strong similarities with the scenarios given by the mode coupling theory of the structural glass transition. [S1063-651X(96)04212-2]

PACS number(s): 82.70.Dd, 78.35.+c, 82.70.Gg, 64.70.Pf

I. INTRODUCTION

Structural relaxation in amorphous systems is an area of much current interest. Many studies have been devoted to the sol-gel transition in systems based on polymers [1–3], natural gelatine [4], and gels based on spherical colloids [5–7]. Here we report on the sol-gel transition in a system of charged *disks* with an aspect ratio of 25, suspended in water. In such systems the orientational degrees of freedom play a crucial role not only in the dynamics but also in the static structure of the gel. Molecular dynamics simulations on hard disk systems reveal a rich phase diagram with nematic and cubatic liquid crystalline phases [8]. However, before these liquid crystalline phases can be formed the system enters a glassy phase or gel. Current opinion favors the “house of cards” structure for the gel [9], which implies a random structure with short range orientational order. On the average the disks are oriented with their positively charged rim towards the negatively charged base of their neighbor. Within this view the orientational degrees of freedom will play a crucial role in the formation of the gel.

Structure and dynamics in the neighborhood of the transition can be studied best by using the noninvasive technique of light scattering, dynamic (DLS) and static. DLS probes the density correlation function describing the time evolution of the density fluctuations. The striking feature, largely emerging from DLS measurements around the gel point [4–6], is the marked similarity of the behavior of the correlation function with the scenarios given by the mode coupling theory of Götze for the structural glass transition in molecular systems [10–13]. In the mode coupling scenarios there are two characteristic algebraic relaxation processes: a faster β relaxation, followed by the slower α relaxation. The relaxation processes are “stretched” towards longer and longer time scales as the transition is approached. In the glass or gel phase only the β relaxation remains, which is

observed as an algebraic decay towards a plateau value. This plateau reflects the onset of structural arrest at the gel point, which is observed as a pure elastic contribution to the scattering, the equivalent of the Debye-Waller factor.

The relevant quantities to be measured are the two algebraic exponents governing the α and β relaxation, and the fraction of frozen-in density fluctuations which is considered the order parameter of the transition. However, an accurate determination of these quantities by light scattering is far from trivial [14]. One of the experimental difficulties encountered is elastic scattering in the gel phase. This static scattering is observed as “speckle” and acts as a spatially fluctuating intrinsic local oscillator. In the intensity correlation function the temporal fluctuations beat to themselves and to the intrinsic static scattering. The density correlation function can be extracted from the intensity correlation function under several assumptions concerning the homogeneity of the sample [15,16]. Secondly, correlation functions measured on gel-like systems exhibit a long-time tail. The integration time used in DLS must extend beyond the longest relaxation time observed, but must be short with respect to the gelation time.

For suspensions of disk-shaped particles called Laponite [17] these conditions can be met and accurate correlation functions can be measured over ten orders in time, as reported here. After preparation the liquidlike suspension evolves in time to form a space filling gel in about 50 h or longer depending on the concentration. During that time we performed DLS measurements and observed the behavior described above, with time as control parameter instead of temperature, density, or volume fraction. This is in contrast to suspensions of spherical colloidal particles where the glass transition was followed as a function of the volume fraction [5,6].

II. LAPONITE RD: PREPARATION AND PARTICLE SIZING

Refined natural and synthetic hectorites and bentonites find a wide industrial application as shear sensitive antisetling agents in water based formulations. The synthetic hec-

*FAX No.: 020-525 5788;

Electronic address: KROON@PHYS.UVA.NL

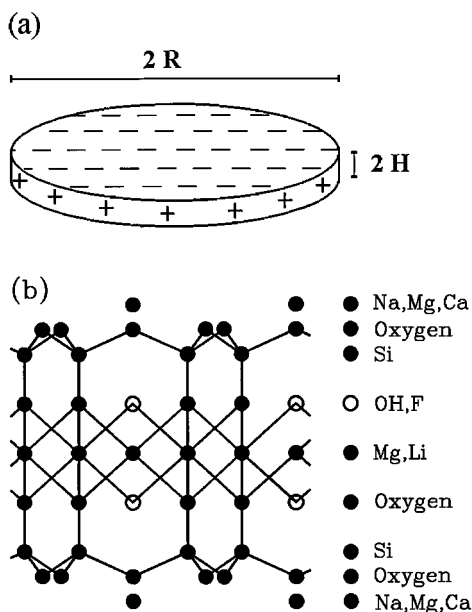


FIG. 1. (a) The disklike shape of the primary Laponite RD particle, and (b) the structure of the primary Laponite particle, as seen from aside (facing the rim). The surface charge distribution as shown in (a) results from the dissolving of surface attached ions (Na, Ca, Mg) into the surrounding liquid. The distribution is fixed due to the crystalline structure of the particle. The legend on the right in (b) displays the elements present in this structure in a horizontal fashion.

torite called Laponite [17] has a number of distinct advantages over natural swelling clays in rheological applications. It is a layered silicate which closely resembles the natural clay mineral hectorite in both structure and composition. It disperses much more easily in water to give colorless, transparent, and highly thixotropic gels. Thixotropy is observed as a fluidlike behavior of the gel when subjected to a shear force above a threshold strength. Laponite is hydrothermally synthesized from simple silicates and lithium and magnesium salts in the presence of mineralizing agents. It is then filtered, washed, dried, and milled.

For our study we have used Laponite RD ($\text{Si}_8[\text{Mg}_{5.5}\text{Li}_{0.4}\text{H}_{4.0}\text{O}_{24.0}]^{-0.7}\text{Na}_{0.7}$) of which the primary particle is shown in Fig. 1(a) (shape) and Fig. 1(b) (structure). Laponite and dust free demineralized water are slowly mixed in a certain mass fraction (1.0–3.5 mass %) and stirred for 2 h with a magnet stirrer. Laponite rapidly disperses in water without heat or shear, which is observed by the disappearance of turbidity. Surface attached ions dissolve into the surrounding liquid. The resulting surface charge distribution remains fixed due to the particle crystal structure. After 10 h the suspension is a charged-stabilized sol, where the light scattering entity is a single Laponite particle [18]. The suspension is filtered using $1\ \mu\text{m}$ filters (Millipore), and poured in a quartz cuvette of 10 mm diameter. As time proceeds we observed the suspensions to show increased viscosity when tumbling the original stock tubes. Finally the suspension behaves as a macroscopically immobile space filling structure which we call the gel. The gel does not flow or adapt its shape when turned in the gravitational field. With the concentrations used no phase separation is observed. The

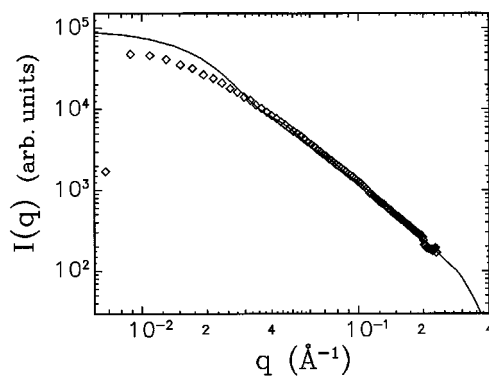


FIG. 2. Comparison of the theoretical form factor $F(\vec{q}, R, H)$ (solid line) for a disk-shaped particle with the small angle x-ray scattering profile as measured on a diluted (1.0 mass %) Laponite suspension in water (diamonds). From this comparison we estimate the particle diameter and thickness to be $2R=25\ \text{nm} \pm 2.5\ \text{nm}$ and $2H=0.9\ \text{nm} \pm 0.1\ \text{nm}$, respectively.

suspensions remain colorless and transparent during gelation and after.

We estimated the single particle dimensions by performing small angle x-ray scattering (SAXS) measurements at the Daresbury Synchrotron Radiation Source on 1.0 mass % suspensions of Laponite in water. These size estimates are obtained by calculating the theoretical expression of the form factor $F(\vec{q}, R, H)$ of a disk-shaped particle with diameter $2R$ and thickness $2H$ [19].

In Fig. 2 we show a comparison of $F(\vec{q}, R, H)$ with the measured SAXS profile from which we estimate $2R=25\ \text{nm} \pm 2.5\ \text{nm}$ and $2H=0.9\ \text{nm} \pm 0.1\ \text{nm}$, with a polydispersity in the diameter of 0.25. The deviation at small scattering vector q is attributed to ordering effects because here q^{-1} is of the same order of magnitude as the interparticle distance. These observations confirm the estimates of Mourchid *et al.* [20], and the results of Avery and Ramsey [21], who studied the rheology of dilute Laponite suspensions.

III. EXPERIMENTAL SETUP

The light scattering setup is shown in Fig. 3. Our primary light source is a cw Ar^+ laser producing 25 mW at a wavelength $\lambda=514.5\ \text{nm}$. The laser beam is focused in the sample to a beam waist of $50\ \mu\text{m}$. The scattered light is detected with a photomultiplier under a fixed scattering angle of 90° in VV polarization. (VV denotes detection of the scattered light with the same polarization as the vertically polarized incoming beam.) The coherence factor $\Psi=0.98$, measured on a dilute sample of latex microspheres, where Ψ^{-1} is the number of speckle spots observed by the detector [22]. The gelation is followed using a gated counter for time-resolved measurements of the scattered intensity, and an ALV-5000 digital correlator [23] for DLS measurements. Each measurement is performed at a randomly chosen position in the sample. To obtain the sample scattered intensity distribution, the sample is slowly ($8\ \mu\text{m/s}$) translated vertically over a distance of 5 mm through the laser beam with a motorized setup, while measuring the scattered intensity.

The progress of the gelation is denoted by the time T

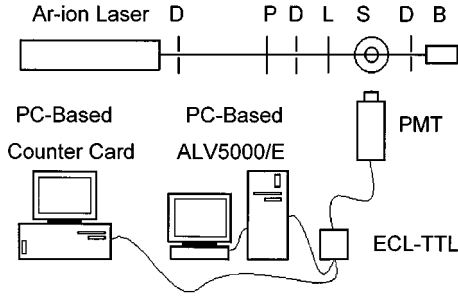


FIG. 3. Plot of the experimental setup. The electronic connections are drawn as curved lines. The optical setup contains several diaphragms (D) defining the beam path, a focusing lens (L), a polarizer (P) which defines the polarization of the incoming light beam, a beam dump (B), and the sample container (S) which contains the sample cuvette in a refractive-index matching bath. The analyzing polarizer is mounted on the detector head (PMT). The sample cuvette (inner circle of S) can be translated vertically through the laser beam with a motorized setup.

where T starts directly after sample preparation. The gelation time T_g is typically of the order of 50 h. We use τ and t to denote time variables associated with the decay of density fluctuations as observed in dynamical measurements. The integration over time t of the time-averaged quantities is continuously increased over the gelation process to efficiently capture the complete spectrum (all time scales) of the fluctuations, and is roughly adjusted to five times the longest correlation time observed in the intensity correlation function. In the gel this is typically 2–4 h. The time scale τ , the time difference argument in the correlation functions, ranges from 10^{-6} to 10^{+3} s.

IV. DYNAMIC LIGHT SCATTERING

In recent years DLS has been applied to systems like colloidal glasses, polymer gels, and clay suspensions. In these systems the local time-averaged properties were observed not to be equal to the sample-averaged properties. The particles in the gel structures are thought to be localized near a fixed time-averaged position around which only small amplitude motions can be executed [15]. The field amplitude $E(t)$ as scattered by the medium undergoing density fluctuations can be written

$$E(t) = E^f(t) + E^c, \quad (1)$$

where the zero-mean complex variable $E^f(t)$ is due to the remaining but restricted particle motion. The static part E^c is scattered off the frozen-in density fluctuations. In the sol phase of the sample this part is absent because here the particle motion is diffusive.

The observed quantity in our scattering experiment is the intensity, defined as $I(t) \equiv E(t)^* E(t)$. The static scattering $I^c \equiv (E^c)^* E^c$ can be found from the time-averaged first and second moment of the intensity distribution [24]. Using Eq. (1) and assuming a Gaussian distribution for $E^f(t)$, one finds

$$\langle I(t) \rangle = \langle I^f(t) \rangle + I^c, \quad (2)$$

$$\langle I(t)^2 \rangle = 2\langle I(t) \rangle^2 - (I^c)^2, \quad (3)$$

where $\langle \rangle$ denotes an average over time t , typically during 2 h. The quantity $\langle I^f(t) \rangle \equiv \langle [E^f(t)]^* E^f(t) \rangle$ denotes the time-averaged fluctuating intensity. For a “fluidlike” sample where the static scattering is absent, one finds $\langle I(t) \rangle = \langle I^f(t) \rangle$ and $\langle I(t)^2 \rangle = 2\langle I(t) \rangle^2$. With Eq. (2) and Eq. (3) we can obtain I^c and $\langle I^f(t) \rangle$ by

$$I^c = [2\langle I(t) \rangle^2 - \langle I(t)^2 \rangle]^{1/2}, \quad (4)$$

$$\langle I^f(t) \rangle = \langle I(t) \rangle - I^c. \quad (5)$$

A single DLS measurement provides an estimate of the time-averaged intensity correlation function $g(\tau)$, defined as

$$g(\tau) \equiv \langle I(t)I(t+\tau) \rangle / \langle I(t) \rangle^2. \quad (6)$$

For sufficiently long delay times τ the system has evolved to a state which is completely uncorrelated with its initial state so that $g(\tau \rightarrow \infty) = 1$. At the shortest delay times $g(\tau \downarrow 0)$ equals the normalized second moment of the scattered intensity. With E^c acting as the intrinsic local oscillator one finds [16]

$$g(\tau) = 1 + x^2 h(\tau)^2 + 2x(1-x)h(\tau). \quad (7)$$

Here $x \equiv \langle I^f(t) \rangle / \langle I(t) \rangle$. The function $h(\tau)$ is the correlation function associated with the fluctuating field component and is defined as

$$h(\tau) \equiv \langle [E^f(t)]^* E^f(t+\tau) \rangle / \langle I^f(t) \rangle. \quad (8)$$

Solving Eq. (7) for $h(\tau)$ results in

$$h(\tau) = 1 + x^{-1} \{ [g(\tau) - g(0) + 1]^{1/2} - 1 \}. \quad (9)$$

In the next section we will experimentally show that the local time-averaged quantities $\langle I^f(t) \rangle$, I^c , and $h(\tau)$ are the relevant quantities with which to describe the sol-gel transition. We will also show that $\langle I^f(t) \rangle$ and $h(\tau)$ are equal to their sample-averaged values. The experimental verification of the homogeneity of the samples for the dynamic properties is an essential condition for both the method presented here and the method presented in [15].

V. RESULTS

A. Results for a 3.0 mass % sample

In Sec. V B we will discuss results obtained with several concentrations ranging from 2.2 to 3.5 mass %. As an example we will here limit the discussion to the results obtained with the 3.0 mass % sample. In Fig. 4 we show the normalized second moment $\langle I(t)^2 \rangle / \langle I(t) \rangle^2$ of the scattered intensity $I(t)$ as a function of time T after sample preparation. At early times the second moment is nearly equal to the ideal value of 2 for a “fluidlike” sample, which shows that the particles are performing “free” Brownian motion. Each data point in Fig. 4 is measured at a different location in the sample.

At a time T_g the smooth behavior changes abruptly into a wide scatter of values. We take this point as the definition of the gelation time. The wide scatter in values stems from the appearance of a speckle pattern, which is the Fourier image of the intrinsic structure of the illuminated sample. The

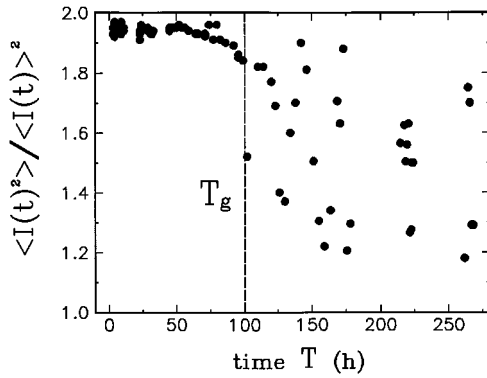


FIG. 4. The time-averaged normalized second moment $\langle I(t)^2 \rangle / \langle I(t) \rangle^2$ of the scattered intensity $I(t)$ as a function of time T after sample preparation. Each point represents an average taken at a different location in the sample. Beyond the dashed line we observe the second moment to abruptly change to a wide scatter of values. This defines the gel point $T_g = 100$ h for this sample.

speckle pattern will change when we illuminate the sample under a different angle or at a different position, since the coherence area is of the order of the width of a speckle spot. The scatter in measured intensities will be of the same order as its average.

Beyond T_g we observe the second moment to be lower than its value of 1.96 as observed in the sol phase. If we now separate the fluctuating and static intensity according to Eq. (4) and Eq. (5) this indicates the presence of a static intensity I^c . In Fig. 5 we show as a function of time T , the static intensity I^c , and the time-averaged fluctuating intensity $\langle I^f(t) \rangle$ obtained with Eq. (4) and Eq. (5). The value of $\Psi = 0.96$ causes the I^c to be nonzero in the sol phase. Beyond the time T_g the smooth behavior of I^c changes to a wide scatter of values, which explains the behavior of the second moment as shown in Fig. 4. It also shows the position dependence of the local oscillator. The results point to the existence of an immobile space filling structure beyond a now well defined T_g . The fast decrease of $\langle I^f(t) \rangle$ just after preparation is assigned to a remnant of the dissolving process of particle clusters into the homogeneous suspension [18]. By eye it is observed as a fading of the initially opaque appear-

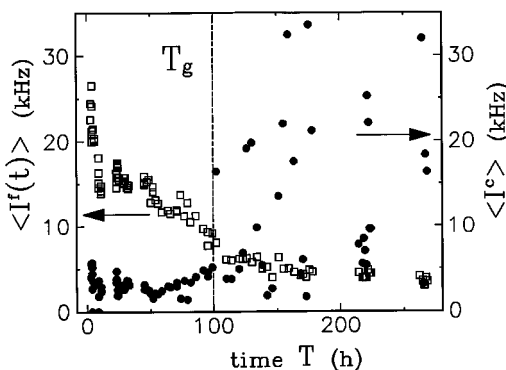


FIG. 5. The fluctuating intensity $\langle I^f(t) \rangle$ (squares) and the static intensity I^c (circles), versus the time T after sample preparation for the 3.0 mass % sample. Note the abrupt change in I^c at the gel point T_g . In this paper we express intensities in terms of the detector count rate (in kHz).

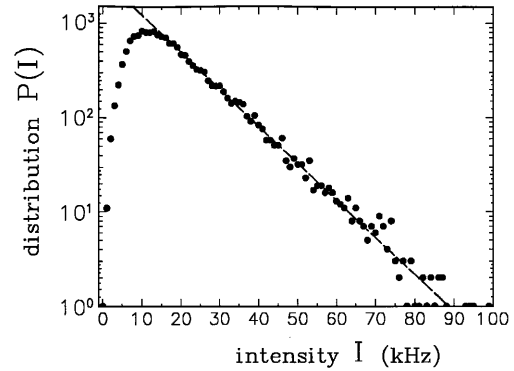


FIG. 6. Distribution $P(I)$ (dots) of the scattered intensity $I(t)$ measured early in the gelation process ($T/T_g = 0.1$) in the 3.0 mass % sample with a gate time of $10 \mu\text{s}$. The dashed line represents a single exponential fit to the distribution given by $A \exp(-I/\langle I \rangle)$ where $A = 3049$, and $\langle I \rangle = 11.03$. It fully represents the fluctuating intensity distribution.

ance. The $\langle I^f(t) \rangle$ remains a smoothly decreasing function of time T , although each data point reflects a measurement at a different location in the sample.

In Fig. 6 we show the distribution of the scattered intensity measured early in the gelation process with a gate time of $10 \mu\text{s}$. The initial upsurge of the distribution and the small horizontal offset are caused by integration over the fastest fluctuations during the gate time. As is clearly seen, we observe a single exponential distribution which is fully attributed to the fluctuating intensity only, because here the second moment is nearly equal to 2. These observations confirm the Gaussian and position independent character of $E^f(t)$, which is assumed to be the case when deriving Eq. (3). The spatial fluctuations in the static intensity (speckle) are uncorrelated with the temporal fluctuations. This observation provides the experimental evidence for the homogeneity of the gel samples for the dynamical properties.

Formally the fraction of frozen-in density fluctuations $f(\infty)$ is defined as the spatially or sample-averaged static intensity normalized to the sample-averaged intensity,

$$f(\infty) \equiv \langle I^c \rangle_s / \langle \langle I(t) \rangle \rangle_s. \quad (10)$$

It is equivalent to the well known Debye-Waller factor, which is considered as the order parameter of the sol-gel transition followed. The $\langle \rangle_s$ denotes an average over the sample. Here we only obtain $\langle \langle I(t) \rangle \rangle_s$ by slow vertical translation of the sample while measuring the scattered intensity with the gated counter. The numerator of Eq. (10) can be rewritten using the observed position independent character of the time-averaged and locally measured $\langle I^f(t) \rangle$. Taking $\langle I^f(t) \rangle = \langle \langle I^f(t) \rangle \rangle_s$, as shown in Fig. 5, we find

$$f(\infty) = 1 - \langle I^f(t) \rangle / \langle \langle I(t) \rangle \rangle_s. \quad (11)$$

In Fig. 7 we show $f(\infty)$ and $\langle \langle I(t) \rangle \rangle_s$ versus the time T after preparation. Each data point results from an average over the sample. Comparing Fig. 7 with Fig. 5 we observe $\langle \langle I(t) \rangle \rangle_s$ and $\langle I^f(t) \rangle$ to show the same dependence on time T at early times. The fast decrease of $\langle \langle I(t) \rangle \rangle_s$ just after preparation is again assigned to a remnant of the dissolving process. Beyond T_g the $\langle \langle I(t) \rangle \rangle_s$ shows minor fluctuations between suc-

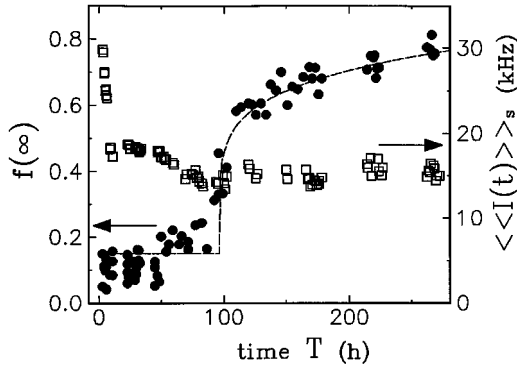


FIG. 7. The sample-averaged intensity $\langle\langle I(t) \rangle\rangle_s$ (squares) and the fraction of frozen-in density fluctuations $f(\infty)$ (circles) versus the time T . The dashed line represents the function $f(\infty) = f_c(\vec{q}) + A[(T - T_g)/T_g]^\varphi$ where $f_c(\vec{q}) = 0.15$, $A = 0.55$, and $\varphi = 0.18$ (see Sec. VI for explanation).

cessive measurements. Here the $\langle I^f(t) \rangle$ and $f(\infty)$ show the same, though mirrored dependence on the time T , which is explained by Eq. (11). In these soft solids it is questionable whether the structure will ever come to full arrest. On time scales an order of magnitude longer than the gelation time, $\langle I^f(t) \rangle$ and $f(\infty)$ have changed minute amounts. They seem to approach values different from 0 and 1, respectively. Just as for glasses, on realistic time scales the gel is considered locally in equilibrium. The remaining temporal fluctuations then originate from intrinsic, collective fluctuations of the gel network.

In Fig. 8 we show an example of the spatial fluctuations in the scattered intensity measured as a function of z , the relative position in the sample, at a time T early (a) and well into the gel phase (b). The counter is gated with a 1 ms integration time. A large part of the temporal fluctuations are integrated over, which results in the offset of the trace in Fig. 8(a). In the gel phase the scattered intensity is dominated by the static part I^c . The scattered intensity pattern as shown in Fig. 8(b) is almost fixed and reproducible. On the walls surrounding the setup it is observed as ‘‘speckle.’’ In Fig. 9 we show the distribution of the scattered intensity as shown in Fig. 8, early (a) and well into the gel phase (b). The distribution is a single exponential function during the entire gelation process, which shows that a sufficient amount of independent scattering volume locations have been visited.

In Fig. 10 we show a typical series of correlation functions $h(\tau)$ as extracted with Eq. (9) from $g(\tau)$ measured at different locations in the sample during the gelation process. The $h(\tau)$ as obtained from measurements on dilute Laponite suspensions consist of a translational and one rotational exponential, because of the disklike shape and cylinder symmetry of the primary particles [22]. For the longest relaxation time we observed a q^2 dependence, where q is the scattering vector, and is thus designated as translational diffusion. The faster relaxation time showed no q^2 dependence and is designated as rotational diffusion. This was verified by measurements on dilute suspensions under VV and VH polarization as a function of the scattering angle. At early times T the intensity scattered on the suspension consists predominantly of a fluctuating term as shown in Fig. 5. Then the ratio $x = 1$ and Eq. (7) reduces to the Siegert relation [22]. As the

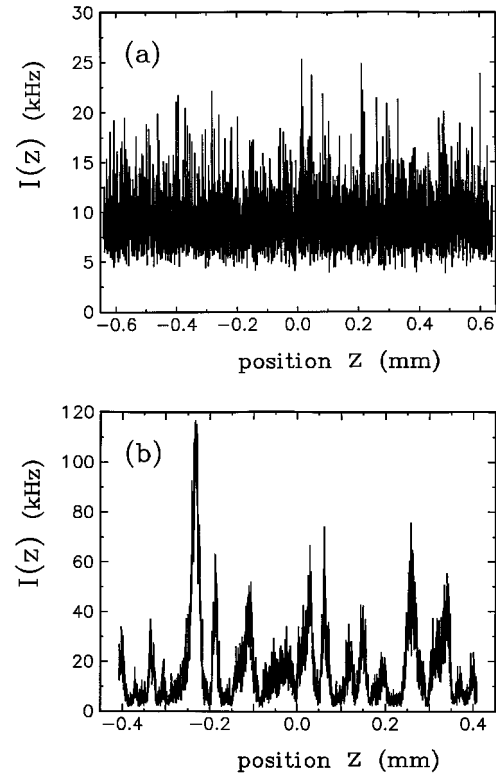


FIG. 8. The scattered intensity $I(z)$ measured as a function of the position z of the scattering volume v in the 3.0 mass % sample early in the gelation [(a) $T/T_g = 0.1$] and far beyond T_g [(b) $T/T_g = 1.8$]. The speckle pattern in (b) is accurately and reproducibly resolved because of the slow scanning speed of $8 \mu\text{m/s}$ and 1 ms gate time.

gelation proceeds we observe the short-time behavior of $h(\tau)$, designated as the rotational diffusion, to be unchanged as verified with cumulant analysis. Apparently the particles in the network formed are allowed to perform free rotational motion around at least one axis. The translational exponential (long-time behavior) shows a stretching over more than five orders in time as the gelation proceeds, until finally the $h(\tau)$ shows a power-law decay τ^{-a} . Beyond T_g we hardly observe changes in $h(\tau)$, although the Laponite system is known to show aging effects [21]. In Fig. 11 we show $h(\tau)$ measured at $T/T_g = 1.7$. Preceded by the unaltered rotational component, we observe a pronounced power-law decay over more than five orders in time τ with a scaling exponent of $a = 0.14 \pm 0.03$.

Beyond the time T_g defined as the transition point, the shape of $g(\tau)$ shows a strong dependence on the position of measurement in the sample, which is explained by the presence of the position dependent static scattering and described by Eq. (3) and Eq. (7). The locally obtained $h(\tau)$ show absolutely no position dependence, which is explained by the position independent character of $E^f(t)$. Hence the locally obtained and time-averaged $h(\tau)$ represents the sample-averaged value $\langle h(\tau) \rangle_s$. Under these conditions Pusey and van Megen [15] already pointed out that one can express the locally obtained and time-averaged $h(\tau)$ in terms of the (sample-averaged) intermediate scattering function $f(\tau)$. The latter is defined as

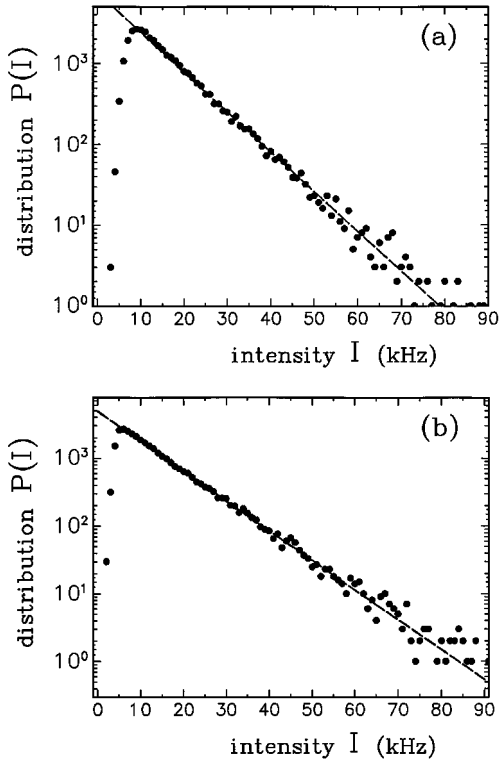


FIG. 9. Distribution $P(I)$ (dots) of the scattered intensity $I(z)$ as shown in Fig. 8. The dashed lines represent a single exponential fit $A \exp(-I/\langle I \rangle)$ with (a) $A=3760$ and $\langle I \rangle=8.80$, and (b) $A=4870$ and $\langle I \rangle=9.89$. The observation of a single exponential distribution ensured a sufficient sampling of independent scattering volume locations.

$$f(\tau) \equiv \langle \langle E(t)E(t+\tau) \rangle \rangle_s / \langle \langle I(t) \rangle \rangle_s. \quad (12)$$

Application of Eq. (1) to Eq. (12) with Eq. (8) yields

$$h(\tau) = \frac{y}{x} [f(\tau) - f(\infty)]. \quad (13)$$

Here $y \equiv \langle \langle I(t) \rangle \rangle_s / \langle I(t) \rangle$ compares the local scattering strength to the sample-averaged scattering strength. With these definitions $x = [1 - f(\infty)]y$.

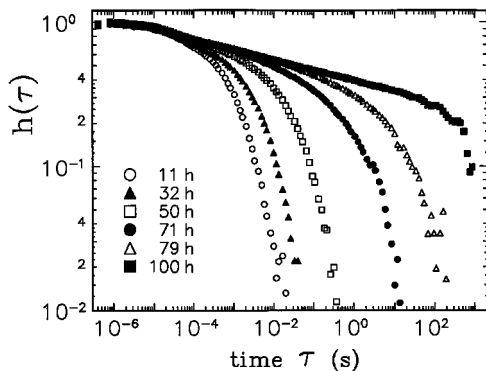


FIG. 10. Typical series of the correlation function $h(\tau)$ as calculated from the measured time-averaged intensity correlation function $g(\tau)$ during the gelation of the 3.0 mass % sample. The legend shows the symbols relating the time T to the measured functions.

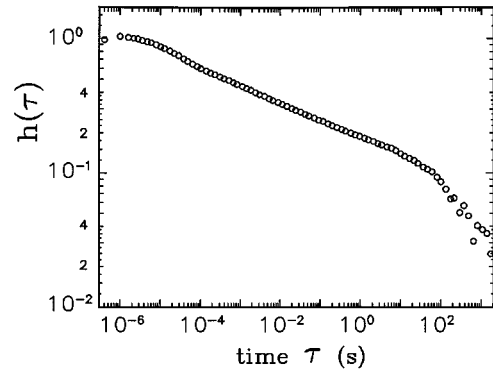


FIG. 11. The correlation function $h(\tau)$ as calculated from $g(\tau)$ measured at $T/T_g = 1.7$ in the 3.0 mass % sample. Preceded by the unaltered rotational component, the $h(\tau)$ shows a pronounced power-law decay τ^{-a} over more than five orders in time τ with a scaling exponent of $a=0.14 \pm 0.03$.

A scaling observed in $h(\tau)$ as extracted from a local observation of $g(\tau)$ will also be observed in $f(\tau) - f(\infty)$. In order to accurately determine the scaling exponent one has to estimate the value $f(\infty)$ with an accuracy of at least 10^{-2} . Otherwise, $f(\tau) - f(\infty)$ can take any desired shape to match to theoretical predictions. In Fig. 12 we show $f(\tau) - f(\infty)$ as extracted from several $g(\tau)$ measured at different locations z in the 2.2 mass % gel with Eq. (9) and Eq. (13). The local oscillator strength is expressed in terms of y . To bring the five depicted functions to overlap over the entire time window, the value of $f(\infty)$ has to be manipulated over more than 3%, which due the double logarithmic scale implies no overlap at all when a fixed estimate of $f(\infty)$ is used.

The accuracy of the sample averaging is hampered by the available spatial range and the finite-time window of averaging against the stability of the setup. Gel-like systems show fluctuations on all time scales and therefore require local averaging times of hours. Approaching the gel point, the intrinsic nonstationarity of the continuously evolving particle system limits the available averaging time to the integration

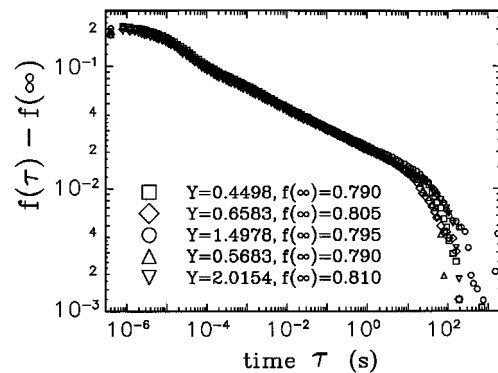


FIG. 12. The sample-averaged intermediate scattering function $f(\tau)$ minus the fraction of frozen-in density fluctuations $f(\infty)$, as extracted from several $g(\tau)$ measured at different locations z in the 2.2 mass % gel at $T/T_g = 2.4$. Note that there are five functions brought to overlap over the entire time window, where the inaccuracy in $f(\infty)$ allows adjustment to obtain optimal overlap. The variation of the local oscillator strength with position z is expressed in terms of y .

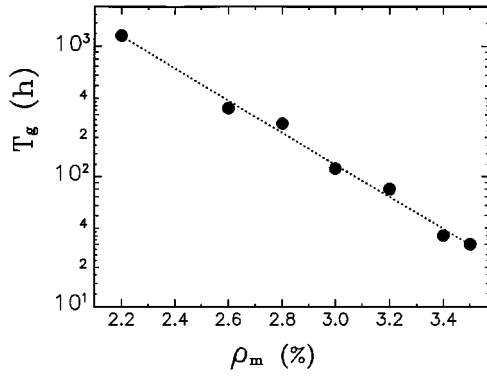


FIG. 13. The gelation time T_g as a function of the mass fraction ρ_m of Laponite in the suspensions investigated. The dashed line represents a single exponential fit according to $T_g \sim \exp(-2.83\rho_m)$.

time used when evaluating local time-averaged properties. Estimating sample-averaged properties with the required accuracy on slowly evolving particle systems is therefore difficult. The method we used here requires no such sample averaging. Apart from the accuracy in the measured $g(\tau)$, the accuracy in determining $h(\tau)$ from $g(\tau)$ is given only by the accuracy in the ratio x . This actually is the precision in the measurement of the second moment $\langle I(t)^2 \rangle / \langle I(t) \rangle^2$ from which the ratio x is calculated. Because the second moment is integrated simultaneously with $g(\tau)$ over at least multiples of the typical correlation time, it will be as accurate as possible to provide us with x .

The method we used here assures the highest accuracy possible in the relevant quantities describing the sol-gel transition.

B. Results for various concentrations

We have also followed the gelation of Laponite suspensions in water at different concentrations or mass fractions ρ_m . Beforehand it was observed that suspensions with a higher mass fraction showed solidification much more rapidly, and one could wonder whether the development of the gelation as set out in Sec. V depends on the specific mass fraction used. The limiting factor in obtaining samples at high concentrations is the inability to fully suspend all clusters of particles before the system shows the phenomenological observation of gelation. The remaining clusters cannot be broken down by forceful stirring. Samples with a concentration lower than 2.0 mass % show a gelation time T_g larger than 2000 h. We therefore limited the study to concentrations in between 2.2 and 3.5 mass %.

The observed behavior of $h(\tau)$, the fluctuating intensity $\langle I^f(t) \rangle$, and the static intensity I^c over the gelation at several concentrations are not different from the results as shown in Fig. 5 and Fig. 10. In all concentrations the $\langle I^f(t) \rangle$ shows a smooth decrease whereas the I^c shows a transition to a wide scatter of values beyond a certain time T_g . The T_g shows a nearly exponential dependence on the concentration ρ_m , as shown in Fig. 13.

This would suggest that the Laponite system does not have a critical concentration ρ_c below which gelation would no longer occur, as argued by Mourchid *et al.* [20]. Fur-

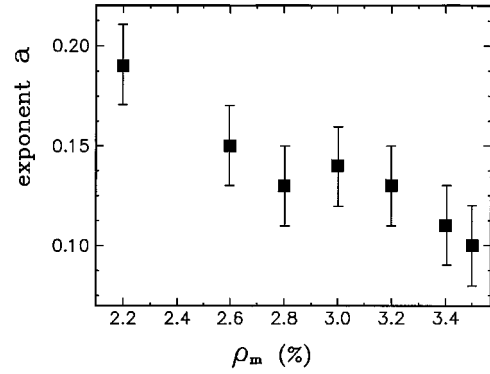


FIG. 14. The scaling exponent a of $h(\tau)$ as a function of the mass fraction ρ_m of Laponite in the suspensions investigated. The scaling exponents and error margins are extracted from a power-law fit to $h(\tau) \sim \tau^{-a}$ in the gel phase of each sample. The exponent a shows a nearly linear relation with ρ_m .

thermore, a stock suspension of 1.0 mass % showed a gel structure after standing alone for at least a year, while no indication for phase separation or density gradients could be found. Therefore the ρ_c is assumed to be small, at least smaller than 0.5 mass %. The scaling exponent of $h(\tau)$ as measured well in the gel phase reveals a surprising and nearly linear dependence on the concentration, as shown in Fig. 14. At higher concentrations the average interparticle distance decreases, thus the interaction strength between particles increases and the gel structure formed is observed to be more rigid. A fluctuating mode is less subject to disturbing thermal fluctuations and shows a less rapid decay of the scaling time correlation.

VI. PREDICTIONS OF MODE COUPLING THEORY

In the past decade the mode coupling theory (MCT) has developed several scenarios for the glass transition. Master curves for the $f(\vec{q}, \tau)$ have been derived, and have been self-consistently calculated for a system of hard spheres [10]. The theory identifies two relaxation processes for glassy systems beyond the region of microscopic motion: α and β relaxation. Close to the glass transition these relaxations span over ten orders in time with well separated time scales τ_α and τ_β . The scaling of these time scales with the control parameter ϵ is different for the two processes, yet interconnected in the theory. The control parameter ϵ that records the distance to the transition point is defined as $\epsilon = (x - x_g)/x_g$ where x is taken as the density, temperature, or volume fraction and x_g its value at the transition. If we take for x the time T , the experimental results show strong similarities with the structural glass transition.

Prior to the glass transition the master curve for $f(\vec{q}, \tau)$ shows a two step decay. First an algebraic decay towards a plateau, β relaxation, followed by the slower α relaxation. Approaching the transition the time window widens until it is stretched to infinity at the transition. After the transition in the gel or glass phase only the β relaxation remains. The $f(\vec{q}, \tau)$ function decays to a plateau, whose value is given by the structure factor at the relevant wave vector and increases as the square root of the distance from the transition point [5,10]. The plateau value is also referred to as the nonergod-

icity parameter or Debye-Waller factor, and is considered as the order parameter for the transition. Close to the transition the mode coupling theory gives the explicit form of $f(\vec{q}, \tau)$ and its scaling behavior. The prevailing scenario for the glass transition gives the following form for the master curve, the relevant algebraic exponents, and their relations:

$$f(\vec{q}, \tau) = f(\vec{q}, \infty) + s(\vec{q}) c_\epsilon g_\pm(\tau/\tau_\epsilon), \quad (14)$$

where $f(\vec{q}, \infty)$ represents the fraction of the structure that is arrested at the transition point ($\epsilon=0$). The amplitude of the β process is $s(\vec{q})c_\epsilon$, with $c_\epsilon = |\epsilon|^{1/2}$, and c_0 is a material dependent constant. The scaling time τ_ϵ diverges with a power of $|\epsilon|$ depending on the process. For the β relaxation the scaling goes as $\tau_\beta = \tau_0 |\epsilon|^{-1/2a}$. For the α process the characteristic time goes as $\tau_\alpha = \tau_0 |\epsilon|^{-\gamma}$ where $\gamma = 1/2a + 1/2b$. The g_\pm function is the master function depending on the rescaled time τ/τ_ϵ only. The subscript \pm indicates the sign of the control parameter ϵ . The explicit expressions are

$$g_-(\tau) = (1/\tau^a) - A_1 \tau^a + A_2 \tau^{3a} + \dots, \quad \tau_\alpha \gg \tau \gg \tau_0$$

$$g_-(\tau) = -B \tau^b + (B_1/B) \tau^b + \dots, \quad \tau_\alpha \gg \tau \gg \tau_\beta \quad (15)$$

where $B > 0$. The nonuniversal exponents a and b , whose values lie in the range of $0 < a < 1/2$ and $0 < b < 1$, are specified by the exponent parameter λ [10]. The exponents are related by the following transcendental equation:

$$\Gamma^2(1+b)/\Gamma(1+2b) = \lambda = \Gamma^2(1-a)/\Gamma(1-2a). \quad (16)$$

The plateau value to which the correlation function decays in the gel phase and which gives the fraction of frozen-in density fluctuations $f_e(\epsilon, \vec{q})$ is predicted to obey [13]

$$f_e(\epsilon, \vec{q}) = f_c(\vec{q}) + \begin{cases} h(\vec{q}) \sqrt{\epsilon} + O(\epsilon), & \epsilon > 0 \\ O(\epsilon), & \epsilon < 0. \end{cases} \quad (17)$$

On the macroscopic time scale $\tau \approx \tau_\alpha$ the dynamics on the fluid side of the transition are governed by the α process. In the glass phase the α process is completely arrested but the β process persists and saturates at long times.

The master function g_\pm is a function of the rescaled time τ/τ_ϵ where τ_ϵ diverges with a power of ϵ depending on the process. As the gelation proceeds towards the gel point T_g , i.e., ϵ approaches zero, the master function preserves its mathematical shape as described by Eq. (15). A practical approach to study the scaling divergence of the slower α relaxation is to follow a certain correlation level of $h(\tau)$ as the gelation proceeds. Basically we draw a horizontal line in Fig. 10 and follow the interception time τ_{inter} of this level with $h(\tau)$. In Fig. 15 we plot τ_{inter} versus $-\epsilon$. Clearly a scaling $\tau_{\text{inter}} \sim |\epsilon|^\xi$ is present at the chosen correlation levels although the scaling exponent ξ ranges from $\xi = -4.6$ for the level $h(\tau) = 0.3$, to $\xi = -6.3$ for the interception with $h(\tau) = 0.03$.

A second practical approach which is widely used to describe the development of $h(\tau)$ is the empirical Kohlrausch function or stretched exponential $F(\tau)$ [5,25],

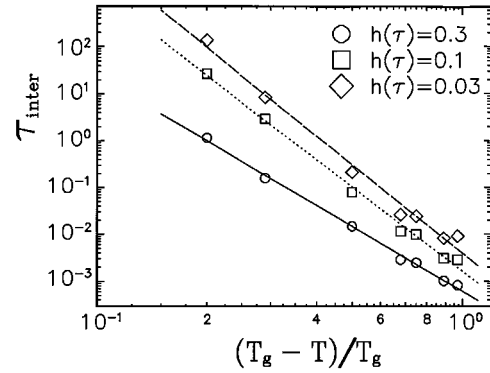


FIG. 15. The interception time τ_{inter} of $h(\tau)$ with several levels of correlation, as a function of $(T_g - T)/T_g$, where $T_g = 100$ h. The legend shows the correlation level at which the interception was followed. The straight lines drawn are power-law fits to the data of which the scaling exponent ranges from -4.6 [solid line, $h(\tau) = 0.3$] to -6.3 [dashed line, $h(\tau) = 0.03$].

$$F(\tau) = A \exp[-(\tau/\tau_z)^\nu]. \quad (18)$$

For certain values of the exponents a and b it is stated that this function accurately describes the master function for the α process. For the hard sphere system the master functions have been calculated numerically [26] and it was found that they could be well parametrized by the Kohlrausch function. In Fig. 10 we showed a typical series of correlation functions $h(\tau)$ as measured during the gelation of the 3.0 mass % sample. As it turned out we were able to match these functions to the empirical Kohlrausch function at times T prior to the gel point T_g , as we show in Fig. 16. The short-time decay of $h(\tau)$ is excluded from the fitting procedure since this part is attributed to the particle rotation. In Fig. 17 we show the typical relaxation time τ_z and scaling parameter ν versus $-\epsilon$. The τ_z reveals a scaling relation with $-\epsilon$, according to $\tau_z = |\epsilon|^{-4.05}$. However, the ν parameter could not be held constant and must be continuously and significantly altered in the vicinity of the gel point T_g . The amplitude A of the Kohlrausch function shows a wide scatter of values which is completely uncorrelated with T or ϵ . Therefore we doubt the applicability of the Kohlrausch function to our data.

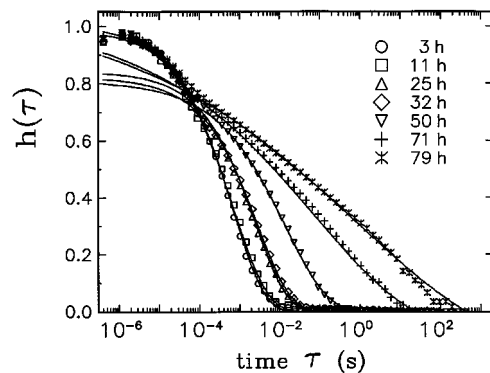


FIG. 16. Matching the empirical Kohlrausch function to the $h(\tau)$ functions as shown in Fig. 10. The solid lines are the fits. The legend shows the symbols related to the time T . Note the scatter of amplitudes at short times τ .

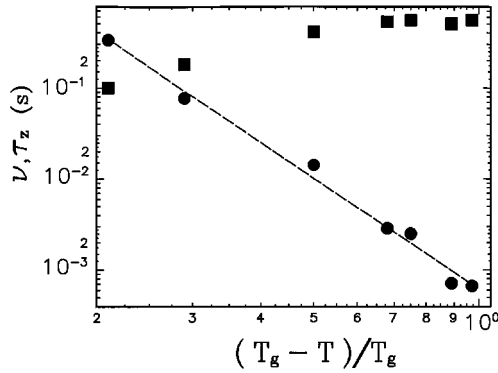


FIG. 17. The time parameter τ_z (circles) and scaling parameter ν (squares) of the empirical Kohlrausch function as a function of the reduced time $(T_g - T)/T_g$, for the functions shown as solid lines in Fig. 16. The dashed curve represents a power-law fit to τ_z according to $\tau_z = K|(T_g - T)/T_g|^{-\phi}$ with $\phi = 4.05$, $K = 6 \times 10^{-4}$ s, where $T_g = 100$ h.

In the gel phase the MCT master function given by Eq. (15) is easily matched to the $h(\tau)$ function when we only take into account the first term of the series expansion. The scaling exponent a of $h(\tau)$ then equals $a = 0.140 \pm 0.03$, and we find a value $\lambda = 0.960 \pm 0.002$ and $b = 0.176 \pm 0.005$. For the scaling exponent of the β and α relaxation we then find $1/2a = 3.58 \pm 0.07$, and $\gamma = 1/2a + 1/2b = 6.42 \pm 0.16$, respectively. Evaluation of τ_{inter} at the higher correlation levels is dominated by the presence of the β relaxation process, while lower levels are likely to be influenced by stability and accuracy. The scaling exponent of τ_z as used in the Kohlrausch function approaches the prediction for the β relaxation time scale best although this estimate is strongly interconnected with the continuously adjusted ν parameter. We therefore conclude that neither practical approach is rigorous in predicting the correct scaling behavior of the diverging time scales.

Finally we tried to match the prediction of MCT on the behavior of the fraction of frozen-in density fluctuations with $f(\infty)$ as presented in Fig. 7. As it turned out we were not able to match $f(\infty)$ with the prediction in the form of Eq. (17). From a power-law fit to $f(\infty) - f_c(\vec{q})$ versus ϵ we observed an exponent ranging from 0.12 to 0.19 for values of $f_c(\vec{q})$ ranging from 0.1 to 0.2. The dashed line in Fig. 7 represents the function $f(\infty) = f_c(\vec{q}) + A[(T - T_g)/T_g]^\varphi$ where $A = 0.55$, $f_c(\vec{q}) = 0.15$, and $\varphi = 0.15$. The smearing of the cusp in the actual measured value of $f(\infty)$ is a discrepancy between theory and the experiment, already pointed out by Li *et al.* [13] and by Götze in [27]. We therefore conclude that our observations are not quantitatively described by the MCT in its idealized form. The $h(\tau)$ functions as measured in the “fluid” region only show qualitative agreement with the predicted behavior.

VII. DISCUSSION

In our study we followed the transition of disklike colloidal system from a well defined “liquid” state (sol) to a “glassy” or gel state. No phase separation is observed to occur for the concentrations considered. A space filling gel

network is formed. The gelation times varied between 50 h to well over a few weeks depending on the concentration. These times are long enough to measure accurate correlation functions during the gelation process, which reveal the mesoscopic dynamics of the system at that specific time point in the gelation process. The correlation functions measured just after the dissolution of Laponite is complete reveal a double exponential shape. These measurements show single Laponite particles undergoing rotational and translational diffusion in a viscous liquid. The moment analysis of the spatial and temporal intensity distributions indicates that this sol evolves into a homogeneous gel. We do not observe the presence of any clusters of particles larger than the single scattering entity.

When the gelation proceeds the faster rotational part remains invariant, while the translational part slows down and becomes independent of the wave vector. Then at least a part of the rotational degrees of freedom is preserved to the single particles even in the gel network. This remaining degree of freedom allows the particles to reorder continuously, and the system to evolve into a more glassy state. Even after the gel has formed the process may continue, albeit at a very much slower pace. Experimentally this is observed in the slow decrease of the algebraic exponent after the gelation time T_g . Thus prior to the sol-gel transition the Laponite system can always be found in some sort of quasiequilibrium state where no frustration is present and then it evolves into the glassy phase.

The physical picture emerging from the correlation functions is a fast local rearrangement of particles followed by the slower collective rearrangement over larger and larger distances. This physical picture and the qualitative features of the correlation functions match rather well with the predictions of mode coupling theory. However, a quantitative description or even a qualitative test of the theory remains out of reach. The difficulty encountered in comparing correlation functions with the predictions of mode coupling theory is the number of free parameters involved in the fitting procedure. For example, it is not possible to test the interconnection of the α and β relaxation. We used mode coupling theory in a pragmatic way as the best phenomenological theory at present in which to present the results. Martin and Wilcoxon [7] proposed a model for the gelation of a polymer gel, which basically considers the gelation as a diffusion limited aggregation process. The stretched exponential function which is then used just does not match our data properly. If one considers an approximate fit enough, the exponents are not constant or relaxation times and amplitudes behave unphysically and inconsistently with the moment analysis. The outcome of the process we sketched is a very fragile glass, where orientational order and/or disorder plays an important part. Preliminary depolarized light scattering and SAXS measurements point that way. There is also evidence from molecular dynamics and Monte Carlo simulations. The transition from an isotropic to a nematic phase is not far off.

Recently an extensive numerical study on a model describing the formation of gels by the Laponite system has been published by Dijkstra *et al.* [28]. When Laponite particles are suspended in water they obtain a negative surface charge and a positive rim charge due to the dissolving of charge balancing ions from the surface of the particles. The

particle interaction is modeled by assigning a quadrupole moment to each of the particles and calculating the orientation dependent interaction. Their results showed a strong dependence on the strength parameter. The symmetry of the interaction used showed a preference for the final structure of the system of many particles to be built up of cubic and triangular building blocks. Although an interesting view on the Laponite particles is presented, the interaction used does not cover the possible complexity of the interaction when the orientation of neighboring particles affects their surface charge distribution or ion cloud structure.

VIII. CONCLUSIONS

We have presented a dynamic light scattering study on the sol-gel transition of a suspension of disk-shaped colloidal particles in water. The measurement of the static part of the scattering combined with the DLS results shows the slowing down of the dynamics of a homogeneous sol until T_g , when a slowly, collectively relaxing network gives rise to the observed speckle pattern. Beyond T_g the sample becomes a space filling macroscopically immobile structure. Provided the gelation process is slow and the dynamics independent of

position in the sample we can derive the true intermediate scattering function from the DLS measurements. From the analysis of the static scattering and the dynamic light scattering results we qualitatively observe many of the characteristics of the glass transition; an algebraic decay in the gel phase, a stretching of the long-time cutoff, and a smeared cusp in $f(\infty)$. Of course, all these quantities make up form and behavior of the intermediate scattering function during the gelation process. However, in the framework of the mode coupling theory we need a multiparameter master function to derive the desired parameters quantitatively. Choice of this function and value of the parameters derived necessarily carry the bias of the user. Even then the results cannot decide between pure β relaxation or the combined α - β relaxation scenario of Götze.

ACKNOWLEDGMENTS

We thank Willem Vos and Ad Lagendijk for stimulating discussions. This research has been supported by the Stichting voor Fundamenteel Onderzoek der Materie (FOM), which is financially supported by the Nederlandse organisatie voor Wetenschappelijk Onderzoek (NWO).

-
- [1] T. Tanaka, L. O. Hocker, and G. B. Benedek, *J. Chem. Phys.* **59**, 5151 (1973).
 - [2] J. G. H. Joosten, E. T. F. Geladé, and P. N. Pusey, *Phys. Rev. A* **42**, 2161 (1990).
 - [3] M. Adam, M. Delsanti, and L. P. Munch, *Phys. Rev. Lett.* **61**, 706 (1988).
 - [4] S. Z. Ren and C. M. Sorensen, *Phys. Rev. Lett.* **70**, 1727 (1993).
 - [5] E. Bartsch, M. Antonietti, W. Schupp, and H. Sillescu, *J. Chem. Phys.* **97**, 3950 (1992).
 - [6] W. van Meegen, S. M. Underwood, and P. N. Pusey, *Phys. Rev. Lett.* **67**, 1586 (1991).
 - [7] J. E. Martin and J. P. Wilcoxon, *Phys. Rev. Lett.* **61**, 373 (1988).
 - [8] J. A. C. Veerman and D. Frenkel, *Phys. Rev. A* **45**, 5632 (1992).
 - [9] H. van Olphen, *Clay Colloid Chemistry*, 2nd ed. (John Wiley, New York, 1977).
 - [10] W. Götze and L. Sjögren, *Phys. Rev. A* **43**, 5442 (1991).
 - [11] E. Leutheusser, *Phys. Rev. A* **29**, 2765 (1984).
 - [12] U. Bengtzelius, W. Götze, and A. Sjölander, *J. Phys. C* **17**, 5915 (1984).
 - [13] G. Li, W. M. Du, J. Hernandez, and H. Z. Cummins, *Phys. Rev. E* **48**, 1192 (1993).
 - [14] X. Zeng, D. Kivelson, and G. Tarjus, *Phys. Rev. Lett.* **72**, 1772 (1994).
 - [15] P. N. Pusey and W. van Meegen, *Physica A* **157**, 705 (1989).
 - [16] J. G. H. Joosten, J. L. McCarthy, and P. N. Pusey, *Macromolecules* **24**, 6690 (1986).
 - [17] Laponite (RD) is manufactured by Laporte Absorbents, P.O. Box 2, Cheshire, UK.
 - [18] D. W. Thompson and J. T. Butterworth, *J. Colloid Interface Sci.* **151**, 236 (1992).
 - [19] A. Guinier and G. Fournet, *Small Angle Scattering of X-rays* (Wiley, New York, 1955).
 - [20] A. Mourchid, A. Delville, A. Lambard, J. Lécolier, and P. Levitz, *Langmuir* **11**, 1942 (1995).
 - [21] R. G. Avery and J. D. F. Ramsey, *J. Colloid Interface Sci.* **109**, 448 (1986).
 - [22] B. J. Berne and R. Pecora, *Dynamic Light Scattering* (Wiley, New York, 1976).
 - [23] K. Schätzel, M. Drewel, and S. Stimac, *J. Mod. Opt.* **35**, 711 (1988).
 - [24] J. W. Goodman, in *Laser Speckle, and Related Phenomena*, edited by J. C. Dainty (Springer-Verlag, New York, 1989).
 - [25] F. Mezei, W. Knaak, and B. Farago, *Phys. Scr.* **19**, 363 (1987).
 - [26] M. Fuchs, I. Hofacher, and A. Latz, *Phys. Rev. A* **45**, 898 (1992).
 - [27] W. Götze, in *Liquids, Freezing and Glass Transition*, edited by J. P. Hansen, D. Levesque, and J. Zinn-Justin (North-Holland, Amsterdam, 1991), p. 464.
 - [28] M. Dijkstra, J. P. Hansen, and P. A. Madden, *Phys. Rev. Lett.* **75**, 2236 (1995).